Thermal annealing of neutron irradiation generated paramagnetic defects in transparent Al_2O_3 ceramics

Andris Antuzevics [a], Edgars Elsts [a], Meldra Kemere [a], Aleksandr Lushchik [b], Aleksandra Moskina [a], Theo A. Scherer [c], Anatoli I. Popov [a,d,*]

[a] Institute of Solid State Physics, University of Latvia, Kengaraga 8, LV-1063, Riga, Latvia
[b] Institute of Physics, University of Tartu, W. Ostwald Str. 1, 50411, Tartu, Estonia
[c] Institut für Angewandte Materialien, Karlsruhe Institute of Technology, Hermann-von-Helmholtz-Platz 1, Eggenstein-Leopoldshafen, 76344, Germany
[d] Department of Technical Physics, L.N. Gumilyov Eurasian National University, Nur-Sultan, 010008, Kazakhstan

Keywords:
Radiation defects
EPR
Luminescence
Thermal annealing
α-Al_2O_3

A B S T R A C T

It is fundamentally important to understand, control, and predict the effect of irradiation on the structure and optical properties of functional materials. In this work, the thermal stability of fast-neutron induced point defects has been investigated in polycrystalline transparent alumina ceramics. The results of a combined study of electron paramagnetic resonance (EPR) and photoluminescence spectroscopy are presented in this paper. The EPR signals related to different trapped-hole centers as well as electron-type F^+ centers have been observed after neutron irradiation. Rapid decay of the total EPR signal intensity occurs after annealing in 600–750 K temperature range. The selective luminescence bands related to the *F*- and F_2-type centers are detected under irradiated corundum ceramics photoexcitation within relevant defect absorption bands (i.e. intracenter excitation/emission).

1. Introduction

α-Al_2O_3 is an important technological material with a wide array of applications such as solid-state lasers, substrates for microelectronics, optical windows, components for fission-based nuclear energetics and corundum is even on the list of promising optical/diagnostics materials for future thermonuclear reactors [1–7]. It is fundamentally important to understand, control, and predict the effect of radiation on the structure and optical properties of functional materials. That is why the study of structural, radiation and optical properties is still so important and attracts the attention of many scientific groups in the world [8–17].

Incident fast neutrons with above-threshold energy cause the displacement of material atoms/nuclei from regular lattice sites into interstices, that is the formation of vacancy-interstitial Frenkel defect pairs, and such collision mechanism solely describes the formation of radiation damage and determines the tolerance of wide-gap metal oxides to harsh radiation environment (see papers [18,19] and references therein). Although the impact mechanism promotes the generation of Frenkel defects in both sublattices of binary/ionic crystals, mainly oxygen-related defects have been studied yet in binary and complex metal oxides.

In particular, the characteristics of the electron-type so-called *F* and F^+ centers an oxygen vacancy with two or one electrons trapped, respectively and their simplest aggregates, F_2-type dimers in different charge states (two, three or four electrons localized within two adjacent oxygen vacancies) have been determined via luminescence and optical absorption spectra of the neutron-irradiated [20–24] and thermochemically reduced α-Al_2O_3 samples [25,26]; in addition, the electron paramagnetic resonance (EPR) signal of the F^+ centers has been revealed in irradiated corundum as well [27,28]. On the other hand, there was a lack of information on single oxygen interstitials complementary centers to the single F-type defects in metal oxides. Only recently the EPR signal of the oxygen interstitial, which is the complementary defect to the F^+ center, has been revealed in neutron-irradiated corundum single crystals and its configuration has been confirmed by the first-principles calculations [29]. Until then, a family of paramagnetic centers holes trapped at oxygen nearby some additional structural defect or impurity (*V* center is often used for the notation of a hole trapped near a cation vacancy) have been detected in binary and complex metal oxides [30–40].

* Corresponding author. Institute of Solid State Physics, University of Latvia, Kengaraga 8, LV-1063, Riga, Latvia.
E-mail address: popov@latnet.lv (A.I. Popov).

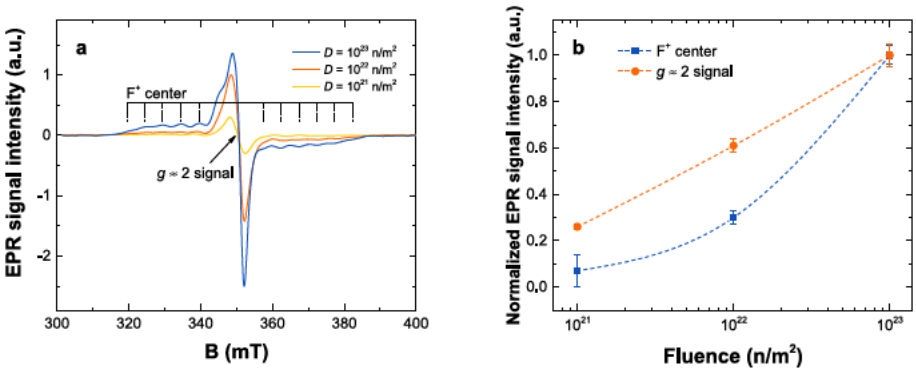

Fig. 1. (a) EPR spectra of Al_2O_3 samples subjected to different neutron fluences; (b) dose dependence of the EPR signal intensity of neutron-induced defects in corundum ceramics before annealing. All spectra were measured at RT, $P = 0.6325$ mW.

Thermal annealing of radiation-induced defects (mainly *F*- and F_2-type centers) has been experimentally studied in Al_2O_3 single crystals via optical absorption and EPR signals [18,23,29,34] and the decay kinetics were analyzed theoretically in terms of diffusion-controlled reactions, applied to other metal oxides as well [34–37,41–43]. Note that the obtained parameters of defect annealing kinetics (activation energy for the diffusion of a mobile recombination component and a corresponding frequency factor) could depend on the type/dose/fluence of radiation, thus allowing to predict the material resistance to heavy irradiation [34,35,37]. On the other hand, the number of studies of intrinsic defect generation and stability in Al_2O_3 ceramics is quite limited.

In the present work, we focus on the creation and further thermal annealing of the F^+ centers and other paramagnetic (mainly trapped-hole) defects accumulated in sintered alumina ceramics under fast-neutron-irradiation with different fluences. It is worth noting that transparent polycrystalline ceramics have several advantages over single crystals including lower cost, easier production, and better mechanical properties [44].

2. Experimental

The alumina transparent ceramic disks were irradiated by fast fission neutrons with energy of $E > 0.1$ MeV and the fluences of 10^{21}, 10^{22} and $10^{23} n/m^2$ (corresponding to about $10^{-4} - 10^{-2}$ dpa) at the High Flux Reactor of the Institute for Advanced Materials of the Joint Research Center (JRC) at Petten.

The samples for EPR and luminescence measurements were cut in cuboids with approximate dimensions of $3 \times 2 \times 1$ mm^3. Stepwise sample thermal annealing was performed in a custom-built tunnel furnace in 400–1000 K range for 10 min at each annealing (preheating) temperature in the air atmosphere. The samples and a thermocouple for temperature monitoring were placed next to each other in an alumina crucible positioned in the center of the furnace. The temperature uncertainty was estimated to be ±10 °C. The relative paramagnetic defect concentration was estimated based on the EPR spectra always measured at the same, room temperature (RT).

All presented EPR spectra were measured at RT with Bruker ELEXSYS-II E500 CW-EPR spectrometer operated at 9.83 GHz microwave frequency. The EPR spectra acquisition parameters were set at 0.3

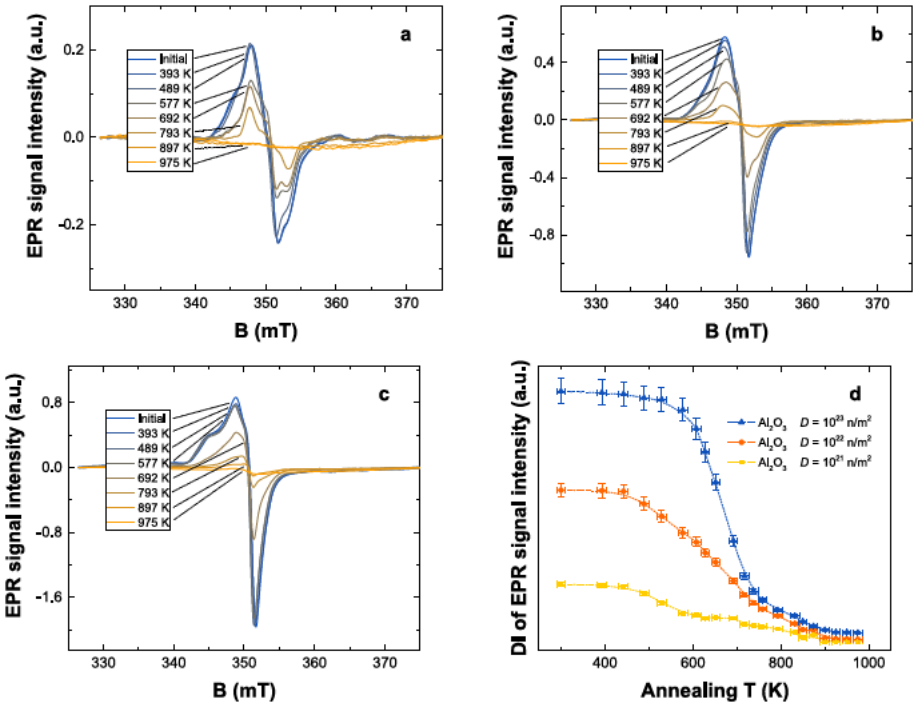

Fig. 2. EPR spectra of samples subjected to neutron fluences of (a) $D = 10^{21}$ n/m^2; (b) $D = 10^{22}$ n/m^2 and (c) $D = 10^{23}$ n/m^2 after annealing at the indicated temperature; (d) DI of EPR signal intensity as a function of the annealing (preheating) temperature. All spectra were measured at RT, $P = 0.6325$ mW.

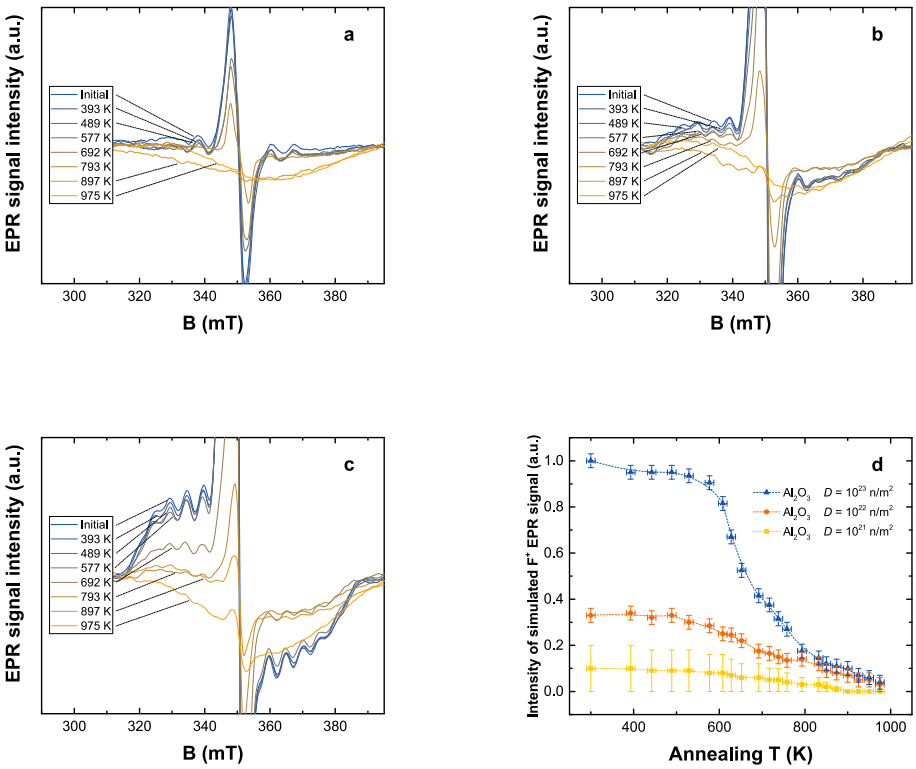

Fig. 3. EPR spectra of the samples subjected to neutron fluences of (a) $D = 10^{21}$ n/m^2; (b) $D = 10^{22}$ n/m^2 and (c) $D = 10^{23}$ n/m^2 (initial) and after additional preheating to the indicated temperatures (the spectra have been zoomed-in to show the contribution of the F^+ signal); (d) decay of the F^+ signal intensity (defect concentration) as a function of preheating temperature. All spectra were measured at RT, $P = 0.06325$ mW.

mT field modulation amplitude and microwave power P 0.6325 mW for the analysis of the full signal at g ≈ 2 mainly associated with different trapped-hole centers (see the next Section for details), while the F^+ electron-type center signal was additionally investigated at 1.5 mT and P 0.06325 mW (optimized conditions for its registration). Each spectrum was averaged across 100 scans, and signal intensities have been normalized to sample mass. EPR spectra simulations have been performed in EasySpin [45]. No probe was used. The cavity quality factor was monitored for all measurements and was determined to be 8000 ± 10% for all measurements.

Photoluminescence emission and excitation spectra were measured at RT using "Edinburgh Instruments" FLS1000-DD-stm Fluorescence Spectrometer equipped with CW 450 W Xenon lamp and cooled red photomultiplier tube for detection. Measurement data were corrected to system sensitivity.

3. Results and discussion

EPR spectra were measured at two different settings (see also Experimental section): the first reflects the overall averaged spectrum from all paramagnetic defects (including, to some extent, a not-optimized weak signal of the F^+ centers) generated by irradiation (will be further called as "$g \approx 2$ signal"); the second was optimized for the selective detection of the F^+ centers. The dependence of paramagnetic defect concentration (proportional to the relevant EPR signal intensity) on fast neutron dose/fluence in the investigated samples before their thermal annealing is presented in **Fig. 1**. The experimental results show clear evidence that electron-type F^+ centers and the defects responsible for the averaged EPR "$g \approx 2$ signal", which are most likely associated with different trapped-hole centers, have different accumulation behavior. The statement related to "$g \approx 2$ signal" origin is based on numerous EPR studies in metal oxides (see e.g., Refs. [20,38,40,46–48]) where EPR signals with g-factor slightly exceeding that for a free electron (g_e 2.0023) are ascribed to a hole localized at regular oxygen ion nearby some additional defect/impurity ion. Note that a rather strict separation of the EPR signals related to two different defect groups (F^+ and trapped hole paramagnetic centers) succeeds due to different P values being used for the registration of these EPR signals (see Figs. 2 and 3).

Fig. 2 shows experimental EPR spectra in the vicinity of $g \approx 2$ (centered around 350 mT) acquired at 0.3 mT field modulation and 0.6325 mW microwave power. Spectra intensities have been normalized to sample mass and, thus, are comparable for the different samples and are proportional to the concentration of paramagnetic defects. EPR signal intensities scale with the neutron dose received by the sample, which provides evidence that the paramagnetic centers are created by neutron irradiation. In oxide materials, spin S 1/2 trapped-hole centers and F^+ centers typically produce resonances in the region of the free electron g_e [20]; however, even in the relatively simple crystal structure of Al_2O_3, the possible defect variations are diverse [38,40,46–48].

It can be inferred from a comparison of spectra shape of the "initial" (before the annealing) samples as well as their evolution during the thermal annealing procedure (the preheating temperatures are given in the figure legends) that several paramagnetic species contribute to the overall spectrum. Precise assignment of the overlapping EPR signals is problematic in non-single crystalline materials; therefore, the superposition of these different signals is referred to as the "$g \approx 2$ signal". Double integral (DI) values of the spectra (that correspond to integral of paramagnetic absorption, i.e., relative defect concentration) in 342–356 mT range were calculated for a quantitative comparison of the "$g \approx 2$ signal" (Fig. 2 d). The most rapid decay of paramagnetic centers occurs after sample annealing in 600–750 K range.

After optimization of EPR spectra acquisition parameters, it was possible to resolve the F^+ center signal; the spectra are shown in Fig. 3. The F^+ -center EPR spectrum at X-band microwave frequency consists of 13 equidistant lines spread over an approximately 70 mT broad field

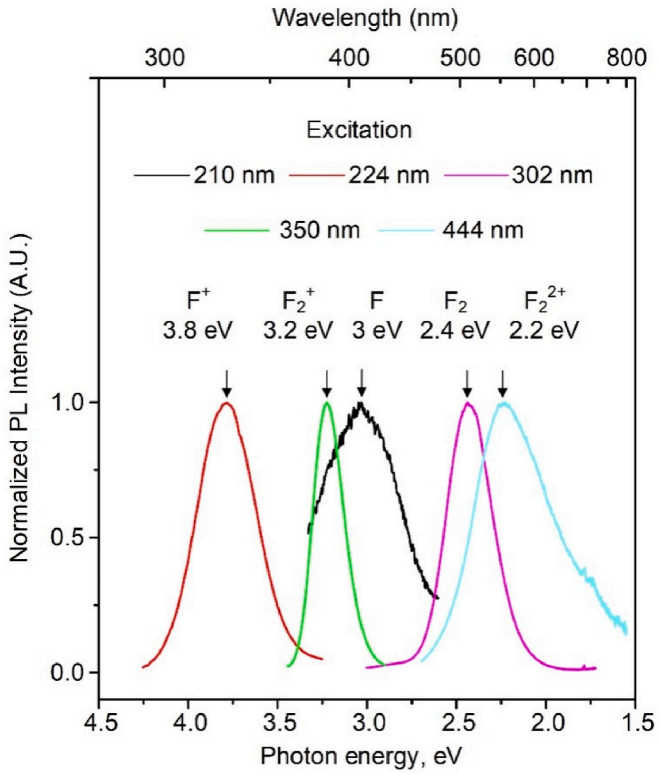

Fig. 4. Normalized PL spectra measured at RT for different excitation energies (the sample was subjected to neutron fluence of $D = 10^{21}$ n/m^2).

region centered around $g \approx 2$. The signal structure originates from S 1/2 (one electron trapped in an oxygen vacancy) hyperfine (HF) interaction with two pairs of slightly inequivalent Al nuclei (100% abundant nuclear spin I 5/2) in the first coordination shells of the center [27–29]. HF structure is clearly resolved for the sample irradiated with the highest dose and can also be discernible for the sample which has received the intermediate dose. For the smallest neutron fluence, there are traces of a broader signal; however, due to poor signal intensity, it is difficult to judge, whether it belongs to the F^+ center. The concentration of the F^+ centers (Fig. 3 d) was estimated from simulations in the EasySpin program; the simulation parameters were taken from paper [27]. Analysis of the EPR signal of the F^+ centers after preheating of the irradiated sample to temperatures above 800 K was problematic due to the poor signal intensity and overlap of broader background signals.

Annealing of the F^+ centers is a multi-stage process with the most rapid decay in 600–800 K range. This result is consistent with experimental studies of neutron and swift-ion irradiated sapphire single crystals [29,37,43,49–51]. Note that in additively colored (thermochemically reduced) sapphire, when only vacancy-related defects are formed, the *F*-type centers remain stable up to about 1300 K [21,25,26]. On the other hand, it is generally accepted that the decay of the F^+ (as well as *F* and F_2-type) centers in the irradiated samples occur due to their recombination with becoming mobile oxygen interstitials (the complementary defect from a radiation-induced vacancy-interstitial Frenkel pair) [18,21,29,33,42,43,51]. Just the latter case is typical of the annealing kinetics of the F^+ centers presented in Fig. 3d. As was already mentioned in the Introduction, annealing kinetics parameters could be dependent on the type and dose of irradiation [34,35,41–43]. However, there are no considerable deviations in the kinetics for the neutron fluence range used in the present study.

The presence of the *F*- and F_2-type centers in neutron-irradiated transparent ceramics has been additionally proved via the spectra of photoluminescence. Fig. 4 presents the emission bands of different single and dimer oxygen-vacancy-related defects ($F^+, F_2^+, F, F_2, F_2^{2+}$ type centers) measured at the excitation of the neutron-irradiated sapphire ceramics by photons with the energies from the region of relevant absorption bands. The defect center peaks in Fig. 4 are normalized because they have different corresponding spectral intensities. Note that such intracenter radiative transitions have thoroughly been studied in α-Al_2O_3 single crystals [21,22,24,26,50–54]. It was mentioned in the literature (see, e.g., papers [25,55]) that the emission of the *F*-centers (peaked at 3 eV) is easily detectable in thermochemically reduced sapphire but is rather weak concerning that in neutron-irradiated samples, where fast (ns-scale) emission of the F^+ centers (3.8 eV) is dominant.

Fig. 5 shows "luminescent fingerprints" of the *F*, F^+, F_2, F_2^+ and F_2^{2+} centers detected in sapphire ceramics irradiated by three different fast neutron fluences. The energies of the exciting photons are indicated in the figure legends. The photoluminescence bands are normalized to illustrate the general picture at different irradiation doses. Although an evident enhancement of defect-related photoluminescence bands with neutron fluence has been detected, a study of the precise dose dependence of defect concentration via photoluminescence characteristics still lies ahead.

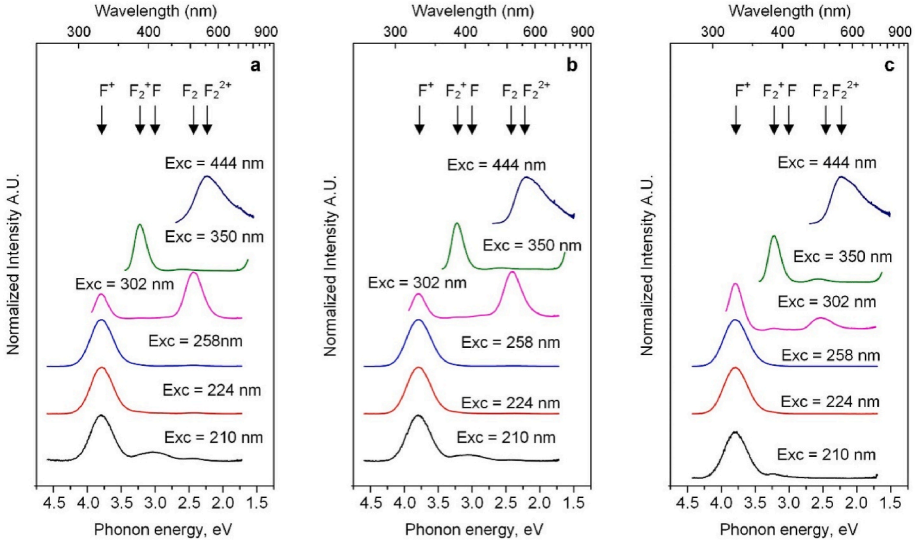

Fig. 5. Emission spectra at different excitation wavelengths measured at room temperature (neutron fluences of (a) $D = 10^{21}$ n/m^2; (b) $D = 10^{22}$ n/m^2 and (c) $D = 10^{23}$ n/m^2).

4. Conclusions

Transparent polycrystalline α-Al_2O_3 ceramics subjected to different neutron fluences have been characterized by the EPR and photoluminescence spectroscopy techniques. The paramagnetic defects generated by fast neutrons have been identified as the electron-type F^+ centers and a set of different undivided hole-trapped centers responsible for the averaged EPR "$g \approx 2$ signal". The F^+ centers are formed at relatively higher neutron fluences, while as-grown structural defects are tentatively also involved in the formation of hole-trapped centers at low irradiation doses. The most rapid thermal annealing of the radiation-induced paramagnetic defects in transparent ceramics occurs in 600–750 K range, which is comparable to that in α-Al_2O_3 single crystals. A set of luminescence bands typical of the *F*- and F_2-type point structural defects has also been detected at the photoexcitation of neutron-irradiated sapphire ceramics in the region of relevant absorption bands.

CRediT authorship contribution statement

Andris Antuzevics: Formal analysis, Data curation, Investigation, Validation, Writing - original draft. **Edgars Elsts:** Investigation, Validation. **Meldra Emere:** Investigation. **Aleksandr Lushchik:** Writing – review & editing. **Aleksandra Moskina:** Methodology. Figures drawing. **Theo A. Scherer:** Supervision. Validation. **Anatoli I. Popov:** Conceptualization, Formal analysis, Funding acquisition, Project administration, Supervision, Writing - review & editing.

Declaration of competing interest

The authors declare that they have no known competing financial interests or personal relationships that could have appeared to influence the work reported in this paper.

Data availability

Data will be made available on request.

Acknowledgements

This work has been carried out within the framework of the EUROfusion Consortium, funded by the European Union via the Euratom Research and Training Programme (Grant Agreement No. 101052200 EUROfusion). Views and opinions expressed are however those of the author(s) only and do not necessarily reflect those of the European Union or the European Commission. Neither the European Union nor the European Commission can be held responsible for them. AIP and AL are also grateful for the support from the COST Action CA17126 (TUMIEE).

References

[1] P. Moulton, Ti-doped sapphire: tunable solid-state laser, Opt News 8 (6) (1982), 9-9.
[2] D.C. Harris, A peek into the history of sapphire crystal growth, Wind. Dome Technol. VIII (5078) (2003) 1–11.
[3] F. Bechtold, A Comprehensive Overview on Today's Ceramic Substrate Technologies, Microelectron. Packag. Conf. Rimini, Italy, 2009, pp. 1–12.
[4] B.S. Patel, Z.H. Zaidi, The suitability of sapphire for laser windows, Meas. Sci. Technol. 10 (3) (1999) 146.
[5] E.R. Dobrovinskaya, L.A. Lytvynov, V. Pishchik, Application of sapphire, Sapphire (2009) 1–54.
[6] S.J. Zinkle, C. Kinoshita, Defect production in ceramics, J. Nucl. Mater. 251 (1997) 200–217.
[7] S.M. Gonzales de Vicente, E.R. Hodgson, T. Shikama, Defect production in ceramics, Nucl. Fusion 57 (2017), 092009.
[8] E.A. Kotomin, A.I. Popov, A. Stashans, A novel model for F^+ to *F* photoconversion in corundum crystals, J. Phys. Condens. Matter 6 (1994) L569–L573.
[9] J.M. Garcia, M. González, M. Roldán, F. Sánchez, The microstructural in-sight to the mechanical behavior of alumina after high energy proton irradiation, Nucl. Mater. Energy 31 (2022), 101173.
[10] F. Mota, C.J. Ortiz, R. Vila, N. Casal, A. García, A. Ibarra, Calculation of damage function of Al_2O_3 in irradiation facilities for fusion reactor applications, J. Nucl. Mater. 442 (1–3) (2013) S699–S704.
[11] R. Vila, M. Gonzalez, M.T. Hernandez, J. Mollá, The role of C-impurities in alumina dielectrics, J. Eur. Ceram. Soc. 24 (6) (2004) 513–1516.
[12] M.G. Brik, Ab-initio studies of the electronic and optical properties of Al_2O_3: Ti^{3+} laser crystals, Phys. B Condens. Matter 532 (2018) 178–183.
[13] X.-K. Hu, B. Wu, Y. Yang, Y.Y. Yeung, C.-G. Ma, M.G. Brik, An old system revisited: Al_2O_3: Ti^{3+}-microscopic crystal field effects explored by the crystal field and first- principles calculations, J. Alloys Compd. 847 (2020), 156459.
[14] D.W. Yang, M.G. Brik, A.M. Srivastava, C.G. Ma, M. Piasecki, Influence of low-symmetry component of crystal field on gemstones colors: Cr^{3+} in ruby and emerald, J. Lumin. 221 (2020), 117061.
[15] A. Platonenko, D. Gryaznov, A.I. Popov, R. Dovesi, E.A. Kotomin, First principles calculations of the vibrational properties of single and dimer *F*-type centers in corundum crystals, J. Chem. Phys. 153 (13) (2020), 134107.
[16] D.V. Ananchenko, S.V. Nikiforov, S.F. Konev, G.R. Ramazanova, ESR and luminescent properties of anion-deficient α-Al_2O_3 single crystals after high-dose irradiation by a pulsed electron beam, Opt. Mater. 90 (2019) 118–122.
[17] V.A. Skuratov, Luminescence of LiF and α-Al_2O_3 crystals under high density excitation, Nucl. Instrum. Methods B. 146 (1–4) (1998) 385–392.
[18] G.P. Pells, Radiation damage effects in alumina, J. Am. Ceram. Soc. 77 (2) (1994) 368–377.
[19] K. Nordlund, S.J. Zinkle, A.E. Sand, F. Granberg, R.S. Averback, R.E. Stoller, T. Suzudo, L. Malerba, F. Banhart, W.J. Weber, F. Willaims, S.L. Dudarev, D. Simeone, Primary radiation damage: a review of current understanding and models, J. Nucl. Mater. 512 (2018) 450–479.
[20] A.E. Hughes, B. Henderson, Color Centers in Simple Oxides, Point Defects in Solids, Springer, Boston, 1972, pp. 381–490.
[21] B.D. Evans, A review of the optical properties of anion lattice vacancies, and electrical conduction in α-Al_2O_3: their relation to radiation-induced electrical degradation, J. Nucl. Mater. 219 (1995) 202–223.
[22] K.H. Lee, J.H. Crawford, Luminescence of the *F* center in sapphire, Phys. Rev. B 19 (6) (1979) 3217.
[23] K. Atobe, N. Nishimoto, Radiation-induced aggregate centers in single crystal Al_2O_8, M. Nakagawa, Phys. Status Solidi 89 (1) (1985) 155–162.
[24] B.D. Evans, G.J. Pogatshnik, Y. Chen, Optical properties of lattice defects in α-Al_2O_3, Nucl. Instrum. Methods B 91 (1–4) (1994) 258–262.
[25] K.H. Lee, J.H. Crawford, Luminescence of the *F* center in sapphire, Appl. Phys. Lett. 33 (4) (1978) 273–275.
[26] R. Ramirez, M. Tardio, R. Gonzalez, J.E. Munoz Santiuste, M.R. Kokta, Optical properties of vacancies in thermochemically reduced Mg-doped sapphire single crystals, J. Appl. Phys. 101 (12) (2007), 123520.
[27] S.Y. La, R.H. Bartram, R.T. Cox, The F^+ center in reactor-irradiated aluminum oxide, J. Phys. Chem. Solid. 34 (6) (1973) 1079–1086.
[28] R.C. Duvarney, A.K. Garrison, J.R. Niklas, J.M. Spaeth, Electron-nuclear double resonance of the F^+ center in α-alumina, Phys. Rev. B 24 (7) (1981) 3693.
[29] V. Seeman, A. Lushchik, E. Shablonin, G. Prieditis, D. Gryaznov, A. Platonenko, E. A. Kotomin, A.I. Popov, Atomic, electronic and magnetic structure of an oxygen interstitial in neutron-irradiated Al_2O_3 single crystals, Sci. Rep. 10 (1) (2020), 15852.
[30] L.E. Halliburton, L.A. Kappers, Radiation-induced oxygen interstitials in MgO, Solid State Commun. 26 (2) (1978) 111–114.
[31] Y. Chen, M.M. Abraham, Trapped-hole centers in alkaline-earth oxides, J. Phys. Chem. Solid. 51 (7) (1990) 747–764.
[32] S. Dolgov, T. Karner, A. Lushchik, A. Maaroos, S. Nakonechnyi, E. Shablonin, Trapped-hole centers in MgO single crystals, Phys. Solid State 53 (6) (2011) 1244–1252.
[33] V. Seeman, E. Feldbach, T. Karner, A. Maaroos, N. Mironova-Ulmane, A.I. Popov, E. Shablonin, E. Vasil'chenko, A. Lushchik, Fast-neutron-induced and as-grown structural defects in magnesium aluminate spinel crystals with different stoichiometry, Opt. Mater. 91 (2019) 42–49.
[34] E. Kotomin, V. Kuzovkov, A.I. Popov, J. Maier, R. Vila, Anomalous kinetics of diffusion-controlled defect annealing in irradiated ionic solids, J. Phys. Chem. A 122 (1) (2018) 28–32.
[35] A. Lushchik, E. Feldbach, E.A. Kotomin, I. Kudryavtseva, V.N. Kuzovkov, A. I. Popov, V. Seeman, E. Shablonin, Distinctive features of diffusion-controlled radiation defect recombination in stoichiometric magnesium aluminate spinel single crystals and transparent polycrystalline ceramics, Sci. Rep. 10 (1) (2020) 1–9.
[36] G. Baubekova, A. Akilbekov, E.A. Kotomin, V.N. Kuzovkov, A.I. Popov, E. Shablonin, M. Zdorovets, E. Vasil'chenko, A. Lushchik, Thermal annealing of radiation damage produced by swift 132Xe ions in MgO single crystals, Nucl. Instrum. Methods B. 462 (2020) 163–168.
[37] A. Lushchik, V.N. Kuzovkov, I. Kudryavtseva, A.I. Popov, V. Seeman, E. Shablonin, E. Vasil'chenko, E.A. Kotomin, The two types of oxygen interstitials in neutron-irradiated corundum single crystals: Joint experimental and theoretical study, Phys. Status Solidi B (2021), 2100317.
[38] R.T. Cox, Electron, Solid State Commun., Electron spin resonance studies of holes trapped at Mg^{2+}, Li+ and cation vacancies in Al_2O_3, Solid State Commun. 9 (22) (1971) 1989–1992.
[39] C.F. Bauer, D.H. Whitmore, Electron spin resonance studies of holes trapped at Mg2+, Li+ and cation vacancies in Al_2O_3, J. Solid State Chem. 11 (1) (1974) 38–52.
[40] K.H. Lee, G.E. Holmberg, J.H. Crawford, Optical and ESR studies of hole centers in γ-irradiated Al_2O_3, Phys. Status Solidi 39 (2) (1977) 669–674.

[41] E.A. Kotomin, V.N. Kuzovkov, A.I. Popov, R. Vila, Kinetics of *F* center annealing and colloid formation in Al_2O_3, Nucl. Instrum. Methods Phys. Res. Sect. B Beam Interact. Mater. Atoms 374 (2016) 107–110.
[42] V.N. Kuzovkov, E.A. Kotomin, A.I. Popov, Kinetics of the electronic center annealing in Al_2O_3 crystals, J. Nucl. Mater. 502 (2018) 295–300.
[43] A.I. Popov, A. Lushchik, E. Shablonin, E. Vasil'chenko, E.A. Kotomin, A. M. Moskina, V.N. Kuzovkov, Comparison of the *F*-type center thermal annealing in heavy-ion and neutron irradiated Al_2O_3 single crystals, Nucl. Instrum. Methods Phys. Res. Sect. B Beam Interact. Mater. Atoms 433 (2018) 93–97.
[44] S.F. Wang, J. Zhang, D.W. Luo, F. Gu, D.Y. Tang, Z.L. Dong, G.E.B. Tan, W.X. Que, T.S. Zhang, S. Li, L.B. Kong, Transparent ceramics: processing, materials and applications, Prog. Solid State Chem. 41 (1–2) (2013) 20–54.
[45] S. Stoll, A. Schweiger, EasySpin, a comprehensive software package for spectral simulation and analysis in EPR, J. Magn. Reson. 178 (1) (2006) 42–55.
[46] F.T. Gamble, R.H. Bartram, C.G. Young, O.R. Gilliam, P.W. Levy, Electron-spin resonances in reactor-irradiated aluminum oxide, physical review, Phys. Rev. 138 (2A) (1965) A577.
[47] J.H. Crawford, A review of neutron radiation damage on corundum crystals, J. Nucl. Mater. 108 (1982) 644–654.
[48] J. Valbis, N. Itoh, Electronic excitations, luminescence and lattice defect formation in α-Al_2O_3 crystals, Radiat. Eff. Defect Solid 116 (1–2) (1991) 171–189.
[49] M. Izerrouken, Y. Djouadi, H. Zirour, Annealing process of *F*-and F^+-centers in Al_2O_3 single crystal induced by fast neutrons irradiation, Nucl. Instrum. Methods Phys. Res. Sect. B Beam Interact. Mater. Atoms 319 (2014) 29–33.
[50] D.V. Ananchenko, S.V. Nikiforov, V.N. Kuzovkov, A.I. Popov, G.R. Ramazanova, R. I. Batalov, R.M. Bayazitov, H.A. Novikov, Radiation-induced defects in sapphire single crystals irradiated by a pulsed ion beam, Nucl. Instrum. Methods Phys. Res. Sect. B Beam Interact. Mater. Atoms 466 (2020) 1–7.
[51] E. Shablonin, A.I. Popov, G. Prieditis, E. Vasil'chenko, A. Lushchik, Thermal annealing and transformation of dimer *F* centers in neutron-irradiated Al_2O_3 single crystals, J. Nucl. Mater. 543 (2021), 152600.
[52] N. Mironova–Ulmane, M.G. Brik, J. Grube, G. Krieke, M. Kemere, A. Antuzevics, E. Gabrusenoks, V. Skvortsova, E. Elsts, A. Sarakovskis, M. Piasecki, EPR, optical and thermometric studies of Cr^{3+} ions in the α-Al_2O_3 synthetic single crystal, Opt. Mater. 132 (2022), 112859.
[53] V. Seeman, A.I. Popov, E. Shablonin, E. Vasil'chenko, A. Lushchik, EPR-active dimer centers with S 1 in α-Al_2O_3 single crystals irradiated by fast neutrons, J. Nucl. Mater. 569 (2022), 153933.
[54] A. Lushchik, V. Seeman, E. Shablonin, E.A. Kotomin, A.I. Popov, Detection of hidden oxygen interstitials in neutron-irradiated corundum crystals, Opt. Mater. X 14 (2022), 100151.
[55] J.H. Crawford, Recent developments in Al_2O_3 color-center research, Semic, Insula (Florianopolis) 5 (3–4) (1983) 599–620.